Air inlet/outlet arrangement for rotor cooling application of axial flux PM machines

Fawzal, AS, Cirstea, R, Woolmer, T, Dickison, M, Blundell, M & Gyftakis, KN

Original citation & hyperlink:
Fawzal, AS, Cirstea, R, Woolmer, T, Dickison, M, Blundell, M & Gyftakis, KN 2018, 'Air inlet/outlet arrangement for rotor cooling application of axial flux PM machines' *Applied Thermal Engineering*, vol 130, pp. 1520-1529
https://dx.doi.org/10.1016/j.applthermaleng.2017.11.121

DOI 10.1016/j.applthermaleng.2017.11.121
ISSN 1359-4311
ESSN 1873-5606

Publisher: Elsevier

Air Inlet/Outlet Arrangement for Rotor Cooling Application of Axial Flux PM Machines

A. S. Fawzal[a], R. M. Cirstea[b], K. N. Gyftakis[c], T. J. Woolmer[d], M. Dickison[e] and M. Blundell[f].

Abstract

The maximum power and torque of a Permanent Magnet (PM) machine may be limited by its magnets' temperature. An operational temperature above the magnets' threshold may cause demagnetization, particularly under abnormal conditions. For Axial Flux Permanent Magnet (AFPM) machines, the PMs are mounted on its rotor, therefore, one way to regulate the PM temperature is via an appropriate rotor cooling method. Selective designs of air inlet and outlet arrangement have been studied by the Computational Fluid Dynamics (CFD) analysis to assess and compare their flow and cooling capabilities. The new cooling designs were then implemented on a Yokeless and Segmented Armature (YASA) machine for flow experimental validation. Additionally, the cooling performance after the design implementation is analysed via CFD. This paper's proposed cooling method is expected to lead to lower magnet temperatures, thus increased reliability, output power and efficiency.

Keywords

CFD; Axial flux machine; Rotor cooling; Permanent magnet machines; Heat transfer

[a] Faculty of Engineering, Environment & Computing, Coventry University, Coventry, UK.
[b] School of Mechanical, Aerospace and Automotive Engineering, Coventry University, Coventry, UK.
[c] School of CEM and the Centre for Mobility and Transport, Coventry University, Coventry, UK.
[d] YASA Motors Ltd. Yarnton, Oxfordshire, UK.
[e] Faculty of Engineering, Environment & Computing, Coventry University, Coventry, UK.
[f] Centre for Mobility and Transport, Coventry University, Coventry, UK.

1.0 Introduction

One of the most reliable Axial Flux Permanent Magnet (AFPM) machines is the Single Stator Double Rotor (SSDR) type, which has a balanced axial force that reduces the machine structural distortion [1]. This machine type has being adopted in the Yokeless and Segmented Armature (YASA) machine with a combination of surface-mounted permanent magnets on the rotor disc [2]-[3]. Similar to any other electrical machine, the YASA machine's performance is limited by the operating temperature in order to avoid high losses, shorter lifetime and possible machine failures. Thus, a good thermal management is important in sustaining a long machine life and increasing the continuous performance of the motor.

Overheating in an electric motor may lead to several problems: degradation of the insulation materials [4]-[5], increase of the copper resistance [6]-[7], Permanent Magnet (PM) demagnetization [8] and deterioration of the bearing's lubrication [9]-[11]. The increase of the copper resistance as well as the PM demagnetisation will lead to poor efficiency if the operating temperature is exceeding the machine specification. In general, the operating temperature of an electric machine is a balance between the heat generation and the heat removal rate [12]-[13]. Therefore, a good thermal management is required in order to boost the machine performance, increase reliability and avoid machine failure due to degradation [7].

Various cooling strategies have being introduced over the years, in managing the thermal behaviour of an AFPM machine, yet priority was given to the regulation of the stator copper losses. Direct cooling approach has been implemented using liquid by sealing the stator assembly to allow for the liquid to pass through [14], [20]-[21] or the air through the creation of flow ventilation [15]. While in-direct cooling method has also been proposed to create a heat path from; conductive potting material to the liquid cooled frame [16]-[27], copper T-bars on slot windings [17], copper bar on stator iron [18], aluminium water-jacket heat sink sandwiched between two slotted stator

cores [19] and coolant tubes surround the windings [14]. In contrast, limited cooling strategies have been introduced to regulate the iron and PM losses on the rotor, while the main focus has been given on the convective heat transfer on the stator-rotor gap such as [26], [32]-[35].

Currently, the YASA machine has a well-established direct liquid cooling system to counter the losses from the stator [20]-[21]. However, this cooling method alone is not enough to cope with the increasing power demand. Therefore, a secondary cooling method has been proposed to manage the temperature from the rotor and PM losses. An initial cooling method has been studied by attaching fan blades to the rotor disc, thus allowing for the machine inflow generation, that cools the rotor and its magnets during operation [22]. The initial cooling method is consider imperfect as the cooling only subjected to the one side of the rotor assembly.

Recent advances in the area of Computational Fluid Dynamics (CFD) and further improvement of the computer hardware have made it possible to achieve accurate flow and thermal analysis of electrical machines [23]-[36]. The complexity of the rotating flow measurement and high cost of testing makes commercial CFD software packages a great tool to predict the flow behaviour. Extensive study in the heat transfer of the AFPM's rotor by air has been made in the past, yet focus was given to the sealed rotor [17], [27]-[28]and centre inlet – radial outlet configuration [21],[31]-[36]. The current paper pushes the research in this field forward by using extensive CFD simulations as the main tool to explore the validity of utilizing the ambient air to cool the rotor and PMs with various inlet/outlet configurations.

The ultimate aim of this study is to propose a novel inlet and outlet design arrangement for dual rotor cooling applications of an AFPM machine. Several arrangements have been selected for analysis in Section 2.0 and an investigation of their cooling capability is discussed in Section 3.0. The leading design is then implanted on a test motor in Section 4.0. The design implementation was made based on flow behaviour, windage losses and

thermal characteristic with compact packaging (minimize axial length), as the key priority. Finally, the results occurring from the CFD flow results are validated with experimental testing data.

2.0 Design Selection and CFD Setup

The design of the AFPM model has been simplified and only a single side of rotor/magnets cavity of SSDR-AFPM machine has been modelled. The 3D CAD design has been created using SolidWorks 2014, and then imported to STAR-CCM+ v11.04 for the CFD setup. Three designs have been proposed and tested as described below:

a) Design 1 – it is a simple approach where the inlet is introduced on the top and the outlet at the bottom of the cavity system.
b) Design 2 – this design is established based on the rotating motion of the rotor disc, where both the inlet and the outlet are tangential to the cavity circular design.
c) Design 3 – it imitates the conventional centrifugal fan/blower/pump design. This design has an inlet at the centre and outlet tangentially to the cavity system.

The pre-processing time can be reduced by combining all three designs into one single modular design during the CAD stage as shown in Fig. 1. Then, during the CFD setup, the corresponded inlet and outlet ducting can be selected to form the desired design. The three proposed designs are presented in Fig. 1 and the parts that are not used in each individual case are greyed out. The blue arrow indicates the inflow direction, whereas the red arrow the outflow. Moreover, the machine rotation was set towards the counter clockwise direction. The detailed drawing of the CFD model is shown in Fig. 2.

Automated mesh generation of polyhedral cells has been selected in STAR-CCM+ to discretise both fluid and solid (rotor and magnets) domains. The target dimensionless wall distance, y^+ ~1 has been used to find the optimum

first cell distance. This is based on a speed of 6000rpm which is equivalent to the local Reynolds number, Re_θ of 5.96e^5 calculated by (1):

$$Re_\theta = \frac{\omega \cdot R^2}{v} \quad \textbf{(1)} .$$

Where ω is the rotor angular speed, R is the rotor outer radius and v is the kinematic viscosity of ambient air at 26.85ºC (300K). An average mesh cell count of 2.3million has been produced.

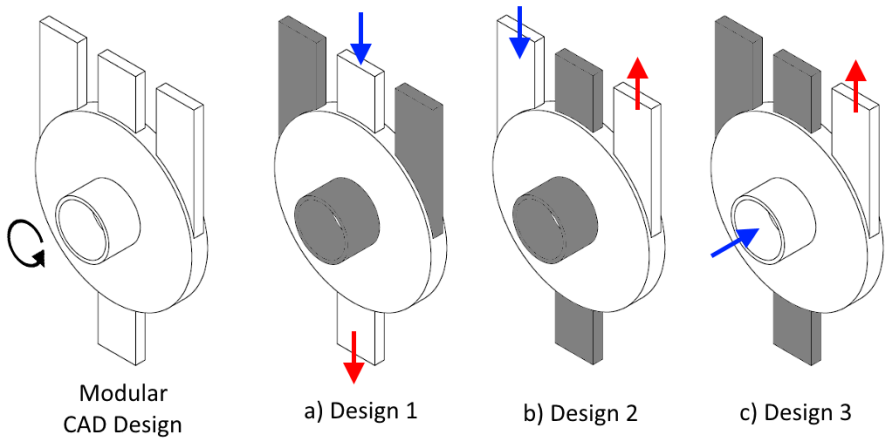

Fig. 1: The CFD model based on modular CAD design that combines all designs and: (a) Design 1 – inlet on top to outlet at bottom, (b) Design 2 – tangential inlet-outlet and (c) Design 3 – conventional centrifugal fan arrangement.

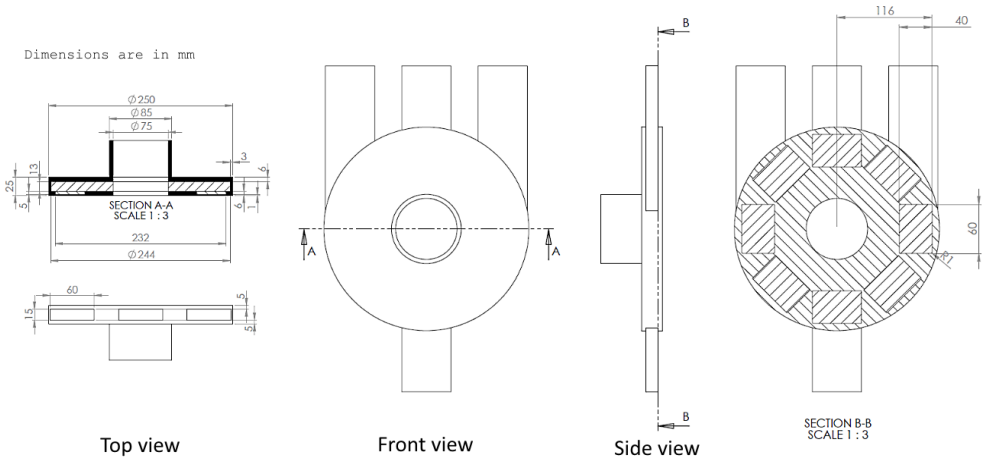

Fig. 2: Detail drawing of the 3D CFD model including section A-A and section B-B.

The fluid domain is separated into two domains, where the domain of the cavity system is set as the rotating domain. This allows for the Moving Reference Frame (MRF) to be set in order to replicate the rotating motion of the rotor/magnets implicitly. On the other hand, the domain of the inlet and outlet remains as a conservative fluid domain. All cavity walls were set at 60ºC and the inlet air temperature of 60ºC is selected to simulate a harsh condition, when the machine operates at extreme thermal stress. The definition of the harsh condition can be such as when the machine is sandwich between the internal combustion engine and the gearbox (for hybridisation) while placed under the vehicle hood (for electric vehicle application or hybridisation) or the operation takes place at hot climates. The inlet and outlet ducting walls are set as adiabatic for simplicity reasons. The inlet boundary mass flow rate for all designs has been set based on the CFD mass flow rate of the backward curved design presented in [22]. The mass flow rate value is expressed by equation (2) below:

$$\dot{m} = 2.895e^{-6} * \left(\left(\frac{60}{2\pi}\right) \cdot \omega\right) - 1.018e^{-3} \quad \textbf{(2)} .$$

The heat generated on the rotor and the magnets in the CFD analysis is set based on the losses that were computed by transient electromagnetic Finite Element Analysis (FEA). The electromagnetic model produced a maximum torque of 375Nm and a speed from 1000rpm to 6000rpm. Fig. 3 illustrates the torque, rotor losses and PM losses corresponding to the rotating speed. The SST (Shear-Stress Transport) k-omega turbulence model [37] is used and the materials' selection for this study is presented in Table 1. The CFD simulation was conducted from 1000rpm to 6000rpm in steps of 1000rpm.

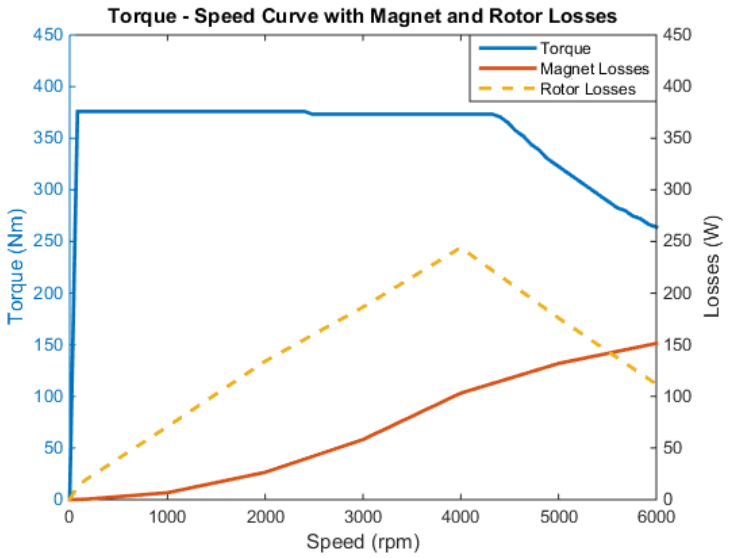

Fig. 3: The torque, rotor losses and magnet losses of a YASA sealed machine produced by FEA.

Table 1: Material Properties

Properties	Air	Rotor	Magnet
Type / Material	Ideal Gas / Air	Solid / Steel	Solid / NdFeB
Dynamic Viscosity (Pa-s)	1.85508E-5	-	-
Molecular Weight (kg/kmol)	28.9664	-	-
Specific Heat (J/kg-K)	1003.6	440.0	490.0
Thermal Conductivity (W/m-K)	0.02603	9.0	48.0
Density (kg/m^3)	-	7500.0	7840.0

3.0 CFD Results and Discussion

The cooling capability of all studied designs can be evaluated by assessing their flow, windage losses and thermal characteristics. The inlet mass flow rate is increased linearly to the speed given by equation (2) for all designs. Therefore, only the pressure difference between the inlet and outlet is assessed.

3.1 Pressure Drop and Windage Losses

The pressure difference between the inlet and the outlet is considered as a pressure drop because the inlet is assumed as stagnation pressure while the outlet is set to the ambient pressure. This assessment is important because an additional ducting will further increase the pressure resistance. Fig. 4 shows the pressure drop of the various designs where Design 1 has the highest pressure drop followed by Design 2 and Design 3. At 6000rpm, Design 1 creates a significant pressure drop and it is 1.20 factors higher than Design 2 and 4.14 factors higher than Design 3. This is because the entry of the Design 1's inlet is straight to the cavity system and this minimizes the suction capability while the rotor assembly is rotating.

Furthermore, the windage losses of all tested designs are shown in Fig. 5 with small difference towards the inlet/outlet design changes. Interestingly, the spinning motion of the rotor in Design 1 is detrimental to the inlet and as a result, this design has slightly higher windage losses followed by Design 3 and Design 2.

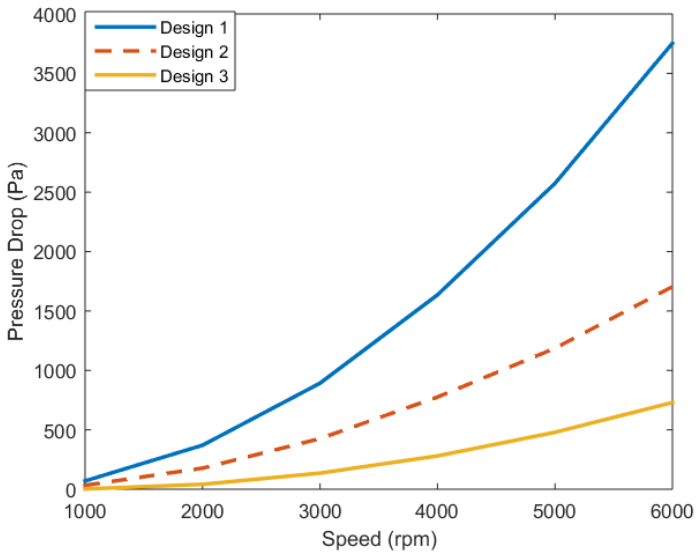

Fig. 4: Pressure drop of the studied designs.

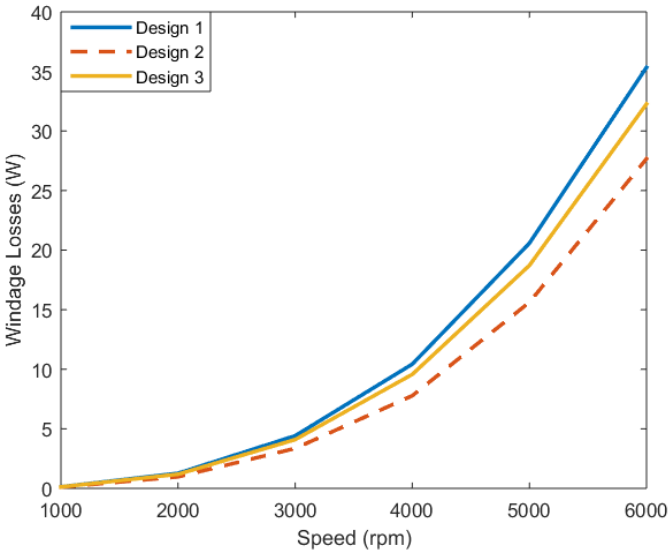

Fig. 5: Windage losses of the studied designs

3.2 Thermal Characteristic

The thermal characteristics produced by all three designs can be assessed by looking at the average temperature of the outlet and within the system cavity. This expresses the ability of the air to absorb the heat from the solid components. Fig. 6 presents the air temperature at the outlet and within the rotational cavity system, where it is clear that the Design 1 has a close relation between air outlet temperature and its cavity system temperature. The Design 2 has an average temperature difference of about 4ºC between the air outlet temperature and its cavity system temperature. On the other hand, the Design 3 has better heat flow out since its outlet temperature is higher than the temperature of the cavity system. This condition can be further appreciated by inspecting the low flow region inside the cavity system. In Fig. 7, the Design 2 has the smallest low velocity region (colour in blue patch of ISO surface) compared to Design 1. In contrast, the Design 3 has covered the whole internal region with the low velocity region, which makes enough absorption rates through heat convention.

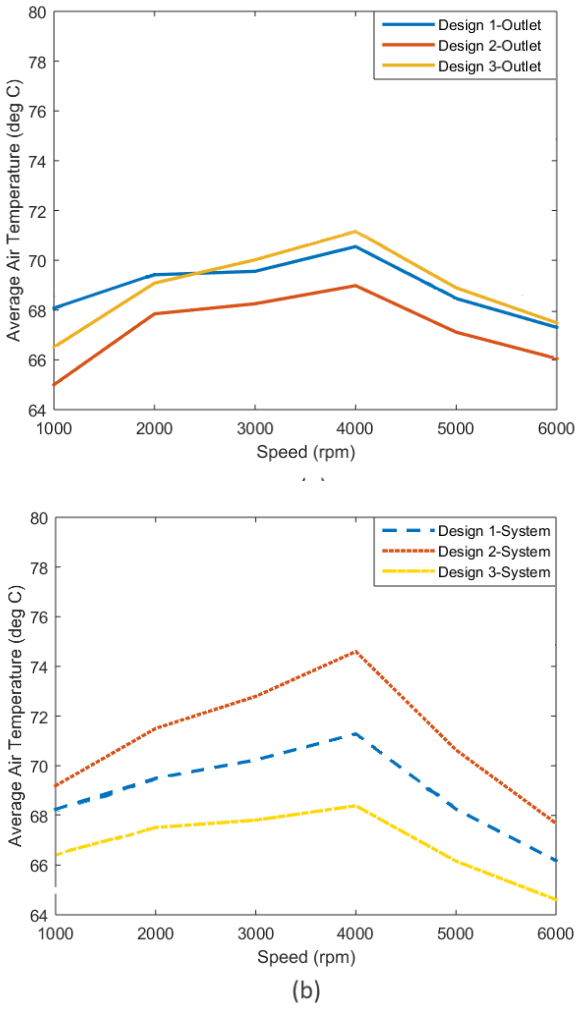

Fig. 6: Average air temperature on (a) the outlet and (b) within the rotational system.

Fig. 8 presents the average temperature of the rotor and the magnet. The peak at 4000rpm of each design is due to the highest input rotor losses at this rotational speed, as presented earlier in Fig. 3. Furthermore, the average heat transfer coefficient is calculated from the results of Fig. 6 and Fig. 8 by equation (3) where *q"* is the heat flux determined by the mass flow rate $\dot{m}$, C_p is the specific heat capacity of air, ΔT is the temperature difference and *A* is the heated area.

$$h_c = \frac{q"}{\Delta T} = \frac{\dot{m} \cdot C_p \cdot (T_{Outlet} - T_{Inlet})}{A \cdot (T_{Rotor} - T_{System})} \quad \textbf{(3)} .$$

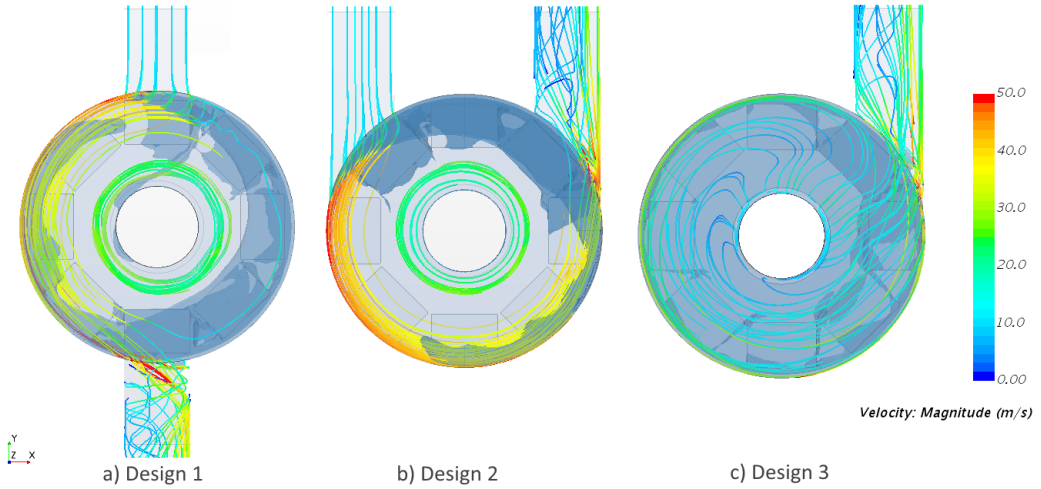

Fig. 7: Flow streamlines of each design and its ISO surface of low velocity region (<10m/s) at 4000rpm in blue translucent patches.

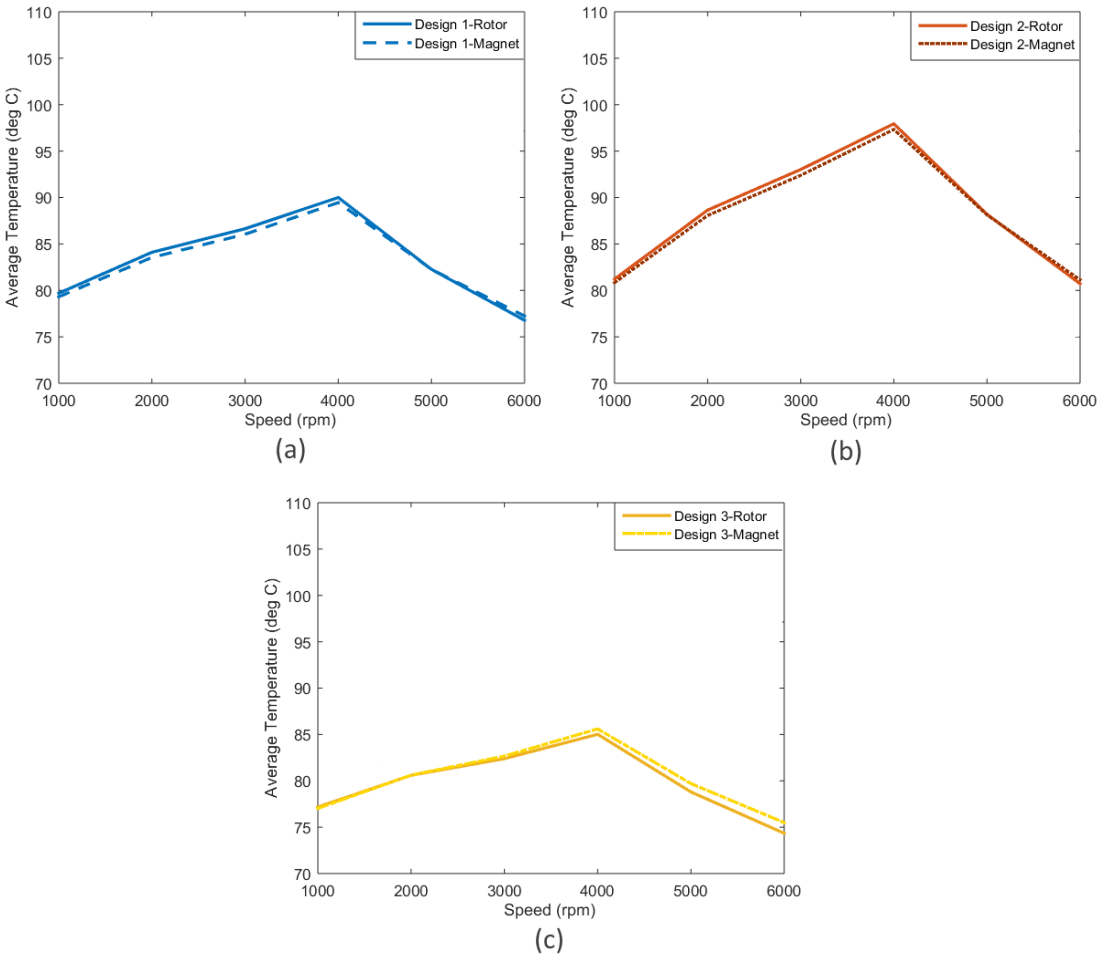

Fig. 8: Average solid temperature of the rotor and the magnets for (a) Design 1, (b) Design 2 and (c) Design 3.

Fig. 9 illustrates that the Design 3 has the best average heat transfer coefficient followed by Design 2 and Design 1. The results are conservative while all designs shared the same mass flow rate value that was specified at the inlet.

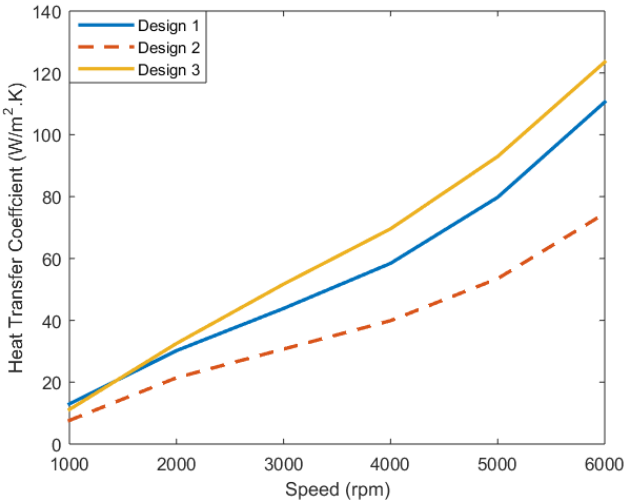

Fig. 9: Average heat transfer coefficient of the studied designs

3.3 Cooling Performance Index (CPI)

In this paragraph, the rotor cooling capability is studied by comparing its convective heat transfer *q,* and the windage losses *W*. The Cooling Performance Index (CPI) was originally proposed in [22] and it is a dimensionless number calculated by the following equation (4).

$$CPI = \frac{Convective\ HT}{Windage\ Losses} \quad \textbf{(4)}\ .$$

The CPI results versus the machine speed are presented in Fig. 10, for the three designs. The major performance difference occurs only at 1000rpm and all shared similar performance at high rotational speed. This means that, regardless of the inlet/outlet design changes, the convective heat transfer is proportionate to its windage losses. Therefore the only selective criterion for the design implementation is based on the difference in the pressure drop of the tested designs.

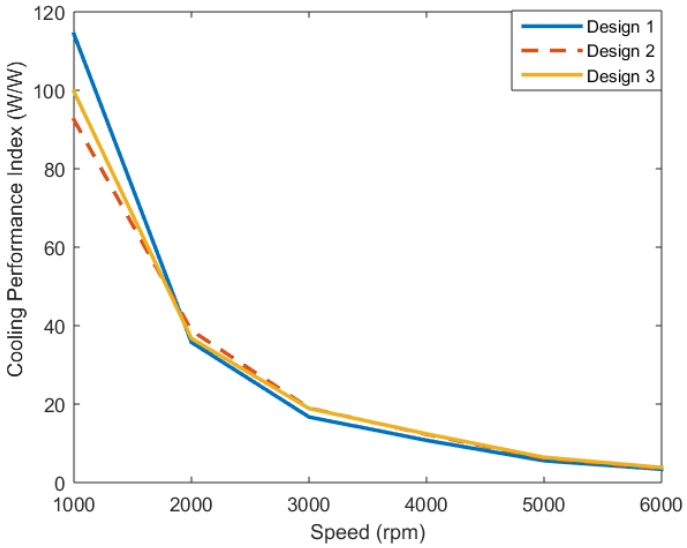

Fig. 10: Cooling Performance Index (CPI) curves of all tested designs.

4.0 Design Implementation

Based on the results presented in the previous section, Design 2 and Design 3 were integrated into the complete assembly of a YASA machine. Design 1 has been discarded because it has produced the highest pressure drop. Fig. 11 shows the CAD for the complete assembly of the proposed design implementation as described below:

a) Design 2 – The tangential inlet and outlet arrangements are adapted on the drive-end (DE) side of the machine. The inlet is channelled from the outlet of Design 3. This is named: ‘DE - Disc side’.
b) Design 3 – The inlet and outlet arrangements are based on a centrifugal fan design and are adapted on the non-drive-end (NDE) side of the machine. A backward curved fan has been attached to the rotor to drive flow in the system. The air outlet of this side will be flow through the inlet of DE side. This is named: ‘NDE - Fan side’.

This new design has increased the YASA machine’s axial length yet it still remains in a tolerable compact packaging thickness. A transfer duct is designed to channel the resulting warm air from the NDE side to the inlet port

of DE side. The resulting hot air is then released to the ambient through the outlet of the DE side.

In Fig. 11, the ducting is coloured in cyan, dark blue is for the fluid domain, red is for the fluid rotational domain and yellow is for the rotors. Two parts not included in the simulations, are the stator in grey colour and the covers in transparent.

To improve clarity, the proposed implementation can be further observed in Fig. 12, which demonstrates the new YASA machine topology integrated with the rotor cooling on both sides. The cool air is drawn in and absorbs heat from the rotor via force convection. As the rotor cools, the heat from the magnets is absorbed by the rotor through conduction. The air from the NDE - fan side was warmed and is then channelled to cool the rotor assembly of the DE - disc side, before exiting to the ambient.

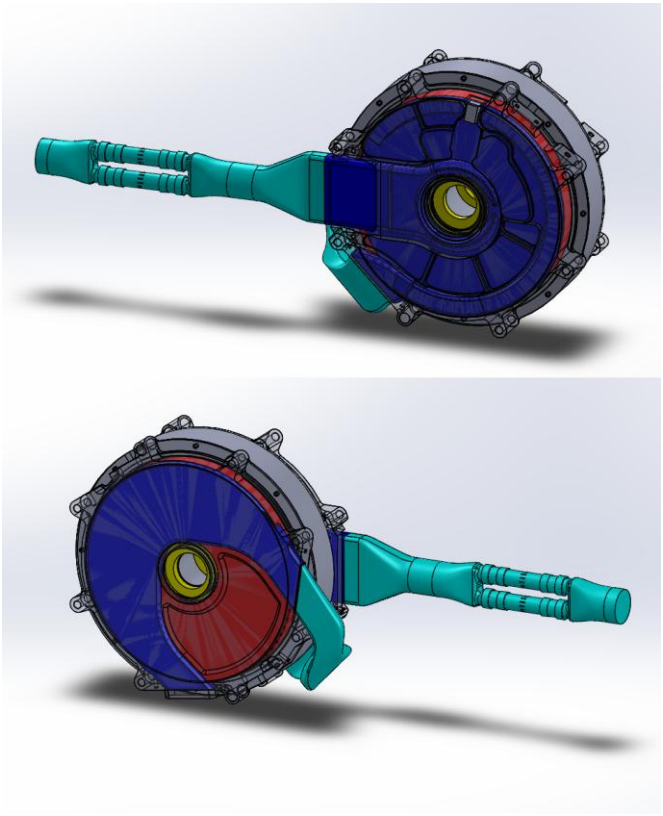

Fig. 11: The YASA machine assembly integrated with Design 2 and Design 3 inlet and outlet arrangement including dual mass flow sensors on the inlet.

The setup such as boundary conditions, losses input and material properties are the same to the ones presented in Paragraph II. The inlet air temperature is set at 26.85ºC (300K). Moreover, no bonding agent is included in this study. In reality a thin layer of adhesive material is present between the magnet and the rotor. The simulations were set to run with a mass flow inlet based on equation (2) for 200 iterations. Later on, they were changed to *stagnation inlet* in order to let the air drawn in by the rotating fan motion of the NDE side until the simulations converge.

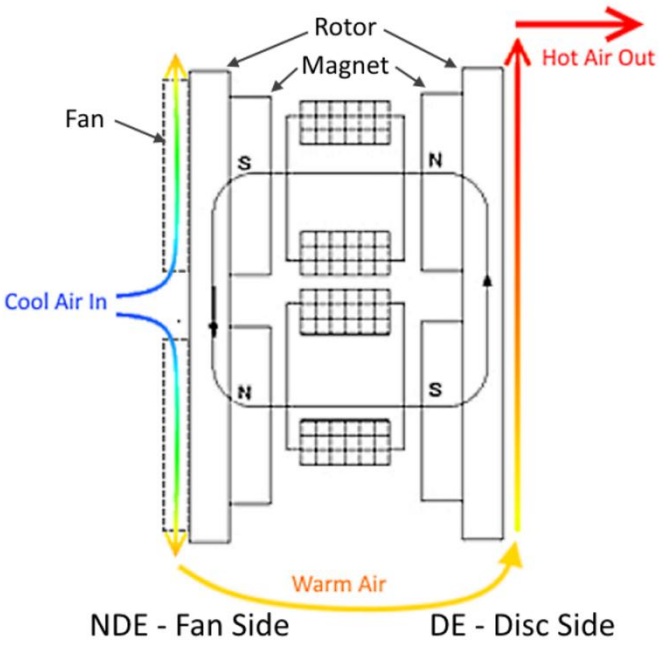

Fig. 12: The new YASA machine topology including rotor cooling on both rotors.

4.1 Experimental Setup

A prototype has been built, according to the CAD design of Fig. 11 and the actual prototype is shown in Fig. 13. The prototype has been built only with the rotor assembly with the magnet arrays attached to it on both sides, while having a blank stator. This allows for the experimental data collection on the flow performance aiming for the mass flow rate to be compared with the CFD results. To perform the measurements, the inlet duct is attached to dual

PMF4104V mass flow sensors. The tested machine is rotated by a secondary motor from 1000rpm to 6000rpm and data have been collected every 1000rpm. Aiming for accurate readings, the machine's speed was held at every 1000rpm.

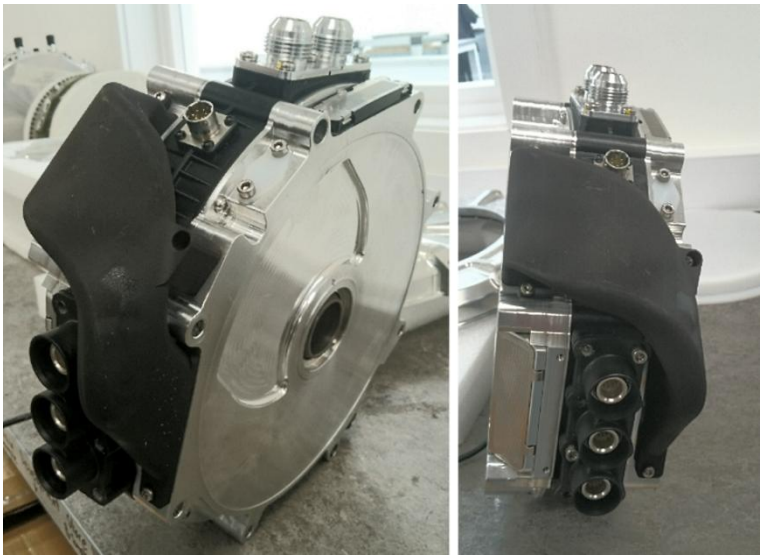

Fig. 13: The prototype of the new YASA machine topology in-cooperate with dual rotor cooling via the air transfer duct.

4.2 Flow validation

The comparison between the CFD simulations and experimentally measured mass flow rates is presented in Fig. 14. The CFD modelling which was conducted by using the SST k-omega turbulence model shows an accurate prediction over the experimental data. The accuracy of CFD modelling was achieved because this study assumed that the whole cavity volume as a rotating fluid region and an only assigned conservative fluid domain to the ducting. This large volume of the rotating region produces a higher mass flow rate because the whole cavity volume implicitly rotates with the fictitious rotating velocity by the MRF method.

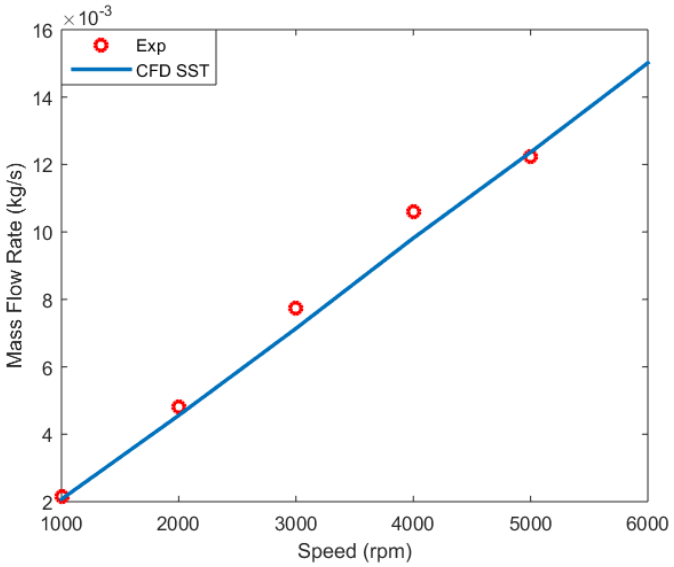

Fig. 14: Comparison between CFD and experimental data of the mass flow rate.

Additionally, the system's pressure rise is extracted from the CFD simulations to estimate if this design implementation may cause stalling effect. The results are shown in Table 2 which led to the conclusion that the combination of Design 2 and Design 3 to the YASA machine produces adequate pressure development without stalling or negative pressure. However, further analysis is required in the special scenario if the intended application requires that the machine will operate under speed less than 1000rpm for a long duration.

Table 2: Pressure rise of dual rotor cooling prototype machine

Speed (*rpm*)	Pressure Rise (*Pa*)
1000	7.98
2000	20.24
3000	49.44
4000	99.46
5000	153.37
6000	229.66

4.3 Thermal Analysis

The average air temperature of the outlet and the cavity system by CFD analysis are shown in Fig. 15. The air flow on the DE - disc side absorbs a significant amount of the heat out, thus its outlet temperature is similar to the

cavity system. This prototype machine has a thin ribs array on DE - disc side rotor surface that disturb the air flow and generate turbulence (Fig. 16-b) which allows for better heat convention. Additionally, greater low velocity patches inside the cavity systems can be observed in the prototype motor (Fig. 16-a) as compared to the initial study.

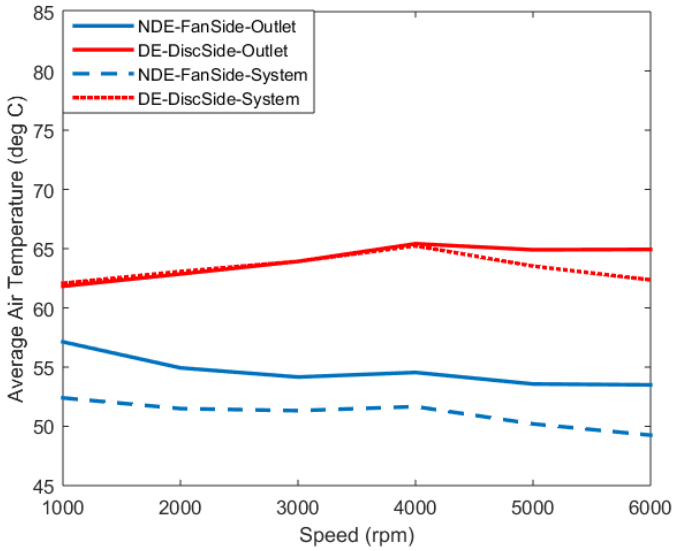

Fig. 15: Average air temperature on the outlet and within the rotational system of the design implementation.

Fig. 17 leads to the fact that the rotor and magnet temperature on the NDE - fan side is lower compared to the DE - disc side as it is expected because the rotor on the fan side has increased surface area and receives cool air from the ambient. The warm air from the NDE - fan side outlet is then channelled and flows to the inlet of the DE - disc side. Consequently the rotor and magnet temperature on DE side is higher. However, the magnet temperature of both rotors is within the generic temperature threshold of NdFeB N00H series magnet at 100°C, as well as the maximum service temperature at 120°C [38].

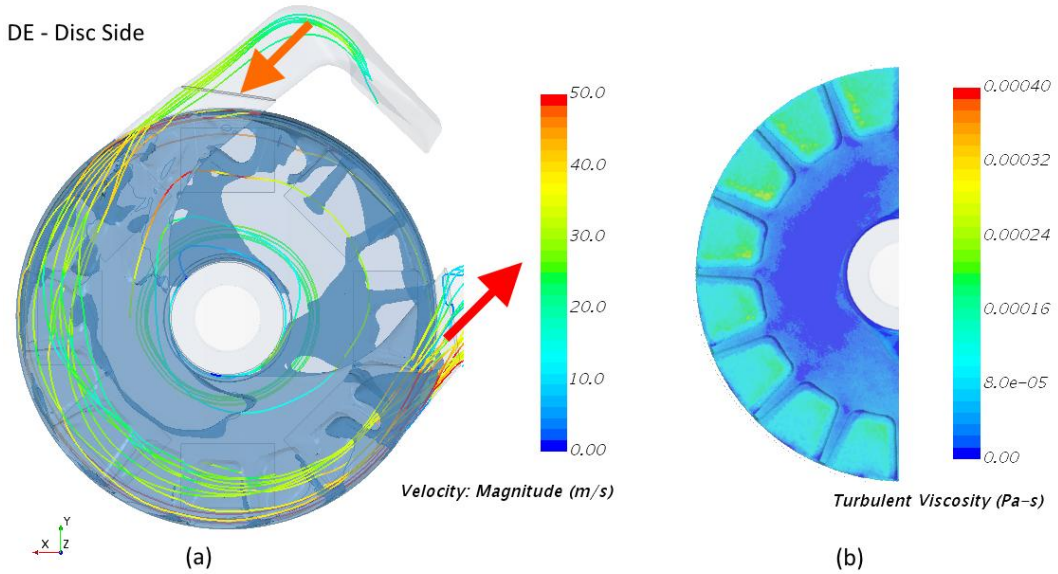

Fig. 16: (a) Flow streamlines and ISO surface of low velocity region (<10m/s) at 4000rpm of DE – disc side. The arrows show the flow direction from ducting. (b) The air turbulence viscosity on the rotor.

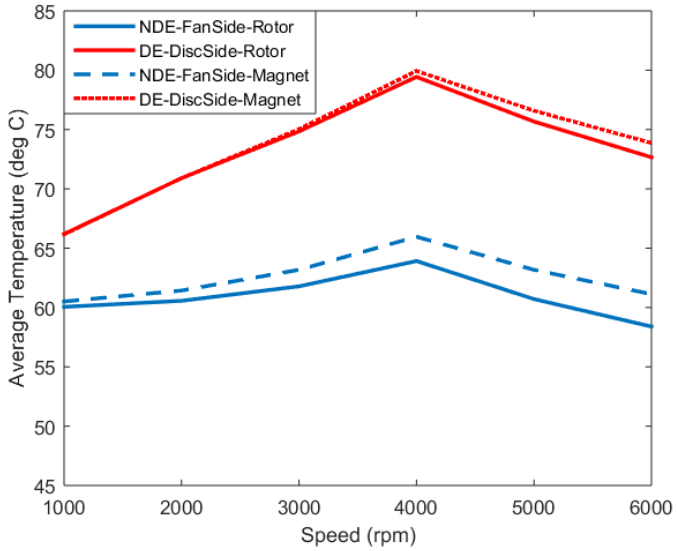

Fig. 17: Average solid temperature of the rotor and the magnets of the design implementation.

5.0 Conclusion

In this paper, a new design concept of different inlet and outlet arrangement method for rotor cooling applications of an AFPM machine by CFD has been presented. Three arrangements are studied and the analysis of each individual design was made by taking advantage of an initial single modular design. This approach has reduced the CAD processing time, where the design can be selected during the CFD pre-processing stage. The proposed methodology can be adopted by any machine designer when dealing with multiple geometrical design cases, which are characterized by a basic geometrical similarity.

The simulated novel inlet and outlet arrangements design were then implemented on a YASA machine to form the dual rotor cooling configuration hence a new topology has been created. The flow results from the design implementation are encouraging where the mass flow rate of the CFD is verified by the experimental data. Moreover, the pressure development of the complete machine assembly shows positive pressure development without any stalling effect.

Furthermore, the thermal analysis in CFD shows that the temperatures of the rotor and permanent magnets have decreased. This will increase the machine reliability and efficiency as it operates under the same load but under lower temperatures than the threshold. Finally, the maximum produced motor output power is further enhanced through the lower operating temperature of the permanent magnets and lower resistance of the stator coils.

Acknowledgment

The authors would like to thank YASA Motor Ltd. Staff especially Chris McCaw, David Mackenzie, Alexander Schnitzler, Tom Hillman and Dr Goh Siew Yan for their support and assistance.

References

[1] C. Chan, "Axial-Field Electrical Machines - Design and Applications", *IEEE Trans. Ener. Conv.*, Vol. 2, No. 2, pp. 294-300, 1987.

[2] T. Woolmer and M. McCulloch, "Axial flux permanent magnet machines: a new topology for high performance applications", *IET Hybrid Vehicle Conference 2006*, 2006.

[3] T. Woolmer and M. McCulloch, "Analysis of the Yokeless And Segmented Armature Machine", *2007 IEEE International Electric Machines & Drives Conference*, pp. 704 - 708, 2007.

[4] K. N. Gyftakis, M. Sumislawska, D. F. Kavanagh, D. A. Howey and M. McCulloch, “Dielectric Characteristics of Electric Vehicle Traction Motor Winding Insulation under Thermal Ageing”, *IEEE Trans. Ind. Appl.,* Vol. 52, No. 2, pp. 1398-1404, 2016.

[5] M. Sumislawska, K. N. Gyftakis, D. F. Kavanagh, M. McCulloch, K. Burnham and D. A. Howey, "The Impact of Thermal Degradation on Properties of Electrical Machine Winding Insulation Material", *IEEE Trans. Ind. Appl.*, Vol. 52, No. 4, pp. 2951-2960, 2016.

[6] M. Laughton and D. Warne, *Electrical Engineer's Reference Book*, 16th ed. Oxford: Elsevier Science, 2003, pp. 5/3-5/4.

[7] W. Tong, *Mechanical design of electric motors*, 1st ed. Virginia: CRC Press, 2014, pp. 1-33, 370-373.

[8] J. Wang, W. Wang, K. Atallah and D. Howe, "Demagnetization Assessment for Three-Phase Tubular Brushless Permanent-Magnet Machines", *IEEE Trans. Magn., V*ol. 44, No. 9, pp. 2195-2203, 2008.

[9] R. Gerstenkorn and T. Somes, "Impacts of Reduced Motor Cooling on Reliability", *IEEE Trans. Ind. Appl.,* Vol. 53, No. 1, pp. 739-744, 2017.

[10] Ying Du, Tonghai Wu and Jun Cheng, "Age detection of lubricating oil with on-line sensors", *2015 IEEE Seneors*, 2015.

[11] T. Harris and M. Kotzalas, *Rolling bearing analysis*, 1st ed. Boca Raton: CRC Press c/o Taylor & Francis, 2007, pp. 451.

[12] Y. Chong, D. Magahy, J. Chick, M. Mueller, D. Staton and A. McDonald, "Numerical modelling of an axial flux permanent magnet machine for convection heat transfer", *IET Conference on Renewable Power Generation (RPG 2011)*, 2011.

[13] D. Kothari and I. Nagrath, *Electric machines*, 4th ed. New Delhi: Tata McGraw-Hill Education, 2010, pp. 250-258.

[14] P. Lindh, I. Petrov, A. Jaatinen-Varri, A. Gronman, M. Martinez-Iturralde, M. Satrustegui and J. Pyrhonen, "Direct Liquid Cooling Method Verified With an Axial-Flux Permanent-Magnet Traction Machine Prototype", *IEEE Transactions on Industrial Electronics*, vol. 64, no. 8, pp. 6086-6095, 2017.

[15] Y. Chong, E. Echenique Subiabre, M. Mueller, J. Chick, D. Staton and A. McDonald, "The Ventilation Effect on Stator Convective Heat Transfer of an Axial-Flux Permanent-Magnet Machine", *IEEE Transactions on Industrial Electronics*, vol. 61, no. 8, pp. 4392-4403, 2014.

[16] M. Polikarpova, P. Lindh, C. Gerada, M. Rilla, V. Naumanen and J. Pyrhönen, "Thermal effects of stator potting in an axial-flux permanent magnet synchronous generator", *Applied Thermal Engineering*, vol. 75, pp. 421-429, 2015.

[17] M. Galea, C. Gerada, T. Raminosoa and P. Wheeler, "A Thermal Improvement Technique for the Phase Windings of Electrical Machines", *IEEE Transactions on Industry Applications*, vol. 48, no. 1, pp. 79-87, 2012.

[18] J. Pyrhönen, P. Lindh, M. Polikarpova, E. Kurvinen and V. Naumanen, "Heat-transfer improvements in an axial-flux permanent-magnet synchronous machine", *Applied Thermal Engineering*, vol. 76, pp. 245-251, 2015.

[19] E. Odvrka, M. Shanel, N. Brown, S. Narayanan, C. Ondruek and A. Mebarki, "Thermal modelling of water-cooled axial-flux permanent

magnet machine", *5th IET International Conference on Power Electronics, Machines and Drives (PEMD 2010)*, 2010.

[20] R. Camilleri, T. Woolmer, A. Court and M. McCulloch, "Investigation into the temperature profile of a liquid cooled YASA© AFPM machine", *6th IET International Conference on Power Electronics, Machines and Drives (PEMD 2012)*, pp. 1-8, 2012.

[21] R. Camilleri, D. Howey and M. McCulloch, "Predicting the Temperature and Flow Distribution in a Direct Oil-Cooled Electrical Machine With Segmented Stator", *IEEE Trans. Ind. Electr*., Vol. 63, No. 1, pp. 82-91, 2016.

[22] A. Fawzal, R. Cirstea, K. Gyftakis, T. Woolmer, M. Dickison and M. Blundell, "Fan performance analysis for rotor cooling of axial flux permanent magnet machines", *IEEE Trans. Ind. Appl., vol. 53, no. 4,* pp. 3295-3304, 2017*.*

[23] P. Moradnia, V. Chernoray and H. Nilsson, "Experimental assessment of a fully predictive CFD approach, for flow of cooling air in an electric generator", *Applied Energy*, vol. 124, pp. 223-230, 2014.

[24] H. Li, "Cooling of a permanent magnet electric motor with a centrifugal impeller", *Int. Jour. of Heat and Mass Transfer*, vol. 53, no. 4, pp. 797-810, 2010.

[25] G. Airoldi, G. Ingram, K. Mahkamov, J. Bumby, R. Dominy, N. Brown, A. Mebarki and M. Shanel, "Computations on heat transfer in axial flux permanent magnet machines", *18th International Conference on Electrical Machines (ICEM 2008)*, pp. 1-6, 2008.

[26] A. Rasekh, P. Sergeant and J. Vierendeels, "Convective heat transfer prediction in disk-type electrical machines", *Applied Thermal Engineering*, vol. 91, pp. 778-790, 2015.

[27] M. Polikarpova, P. Ponomarev, P. Lindh, I. Petrov, W. Jara, V. Naumanen, J. Tapia and J. Pyrhonen, "Hybrid Cooling Method of Axial-Flux Permanent-Magnet Machines for Vehicle

Applications", *IEEE Trans. Ind. Electr*., Vol. 62, No. 12, pp. 7382-7390, 2015.

[28] B. Dong, K. Wang, B. Han and S. Zheng, "High-speed permanent magnet motor with magnetic bearings: Multi-physics analysis, cooling design and experiment", *19th International Conference on Electrical Machines and Systems (ICEMS)*, 2016, 2016.

[29] A. Tuysuz, F. Meyer, M. Steichen, C. Zwyssig and J. Kolar, "Advanced Cooling Methods for High-Speed Electrical Machines", *IEEE Trans. Ind. Appl.,* pp. 1-1, 2017.

[30] T. Nakahama, F. Ishibashi, K. Sato and K. Kawano, "Effects of Fan Blade Forward-Swept and Inclined Amounts in Electric Motors", *IEEE Trans. Ener. Conv.*, Vol. 25, No. 2, pp. 457-464, 2010.

[31] T. Nakahama, K. Suzuki, S. Hashidume, F. Ishibashi and M. Hirata, "Cooling Airflow in Unidirectional Ventilated Open-Type Motor for Electric Vehicles", *IEEE Trans. Ener. Conv.*, Vol. 21, No. 3, pp. 645-651, 2006.

[32] D. Howey, A. Holmes and K. Pullen, "Measurement and CFD Prediction of Heat Transfer in Air-Cooled Disc-Type Electrical Machines", *IEEE Trans. Ind. Appl., V*ol. 47, No. 4, pp. 1716-1723, 2011.

[33] D. Howey, A. Holmes and K. Pullen, "Radially resolved measurement of stator heat transfer in a rotor–stator disc system", *Int. Jour. of Heat and Mass Transfer*, Vol. 53, No. 1-3, pp. 491-501, 2010.

[34] B. Yoheswaran and K. Pullen, "Flow and convective heat transfer in disk-type electric machines with coolant flow", *2014 International Conference on Electrical Machines (ICEM)*, 2014.

[35] A. Rasekh, P. Sergeant and J. Vierendeels, "Fully predictive heat transfer coefficient modeling of an axial flux permanent magnet synchronous machine with geometrical parameters of the magnets", *Applied Thermal Engineering*, vol. 110, pp. 1343-1357, 2017.

[36] C. Lim, G. Airoldi, R. Dominy and K. Mahkamov, "Experimental validation of CFD modelling for heat transfer coefficient predictions in axial flux permanent magnet generators", *Int. Jour. Of Thermal Sciences*, vol. 50, no. 12, pp. 2451-2463, 2011.

[37] F. Menter, "Two-equation eddy-viscosity turbulence models for engineering applications", *AIAA Journal*, vol. 32, no. 8, pp. 1598-1605, 1994.

[38] Eclipse Magnetics, *Sintered Neodymium Iron Boron (NdFeB) Magnets*, 1st ed. Eclipse Magnetics, pp. 3-15.